Meteoritics & Planetary Science 39, Nr 12, 1815–1832 (2003)
Abstract available online at http://meteoritics.org

Melting in the martian mantle: Shergottite formation and implications for present-day mantle convection on Mars

Walter S. KIEFER

Lunar and Planetary Institute, 3600 Bay Area Boulevard, Houston, Texas 77058, USA
E-mail: kiefer@lpi.usra.edu

(Received 23 April 2003; revision accepted 23 December 2003)

Abstract–Radiometric age dating of the shergottite meteorites and cratering studies of lava flows in Tharsis and Elysium both demonstrate that volcanic activity has occurred on Mars in the geologically recent past. This implies that adiabatic decompression melting and upwelling convective flow in the mantle remains important on Mars at present. I present a series of numerical simulations of mantle convection and magma generation on Mars. These models test the effects of the total radioactive heating budget and of the partitioning of radioactivity between crust and mantle on the production of magma. In these models, melting is restricted to the heads of hot mantle plumes that rise from the core-mantle boundary, consistent with the spatially localized distribution of recent volcanism on Mars. For magma production to occur on present-day Mars, the minimum average radioactive heating rate in the martian mantle is 1.6×10^{-12} W/kg, which corresponds to 39% of the Wänke and Dreibus (1994) radioactivity abundance. If the mantle heating rate is lower than this, the mean mantle temperature is low, and the mantle plumes experience large amounts of cooling as they rise from the base of the mantle to the surface and are, thus, unable to melt. Models with mantle radioactive heating rates of 1.8 to 2.1×10^{-12} W/kg can satisfy both the present-day volcanic resurfacing rate on Mars and the typical melt fraction observed in the shergottites. This corresponds to 43–50% of the Wänke and Dreibus radioactivity remaining in the mantle, which is geochemically reasonable for a 50 km thick crust formed by about 10% partial melting. Plausible changes to either the assumed solidus temperature or to the assumed core-mantle boundary temperature would require a larger amount of mantle radioactivity to permit present-day magmatism. These heating rates are slightly higher than inferred for the nakhlite source region and significantly higher than inferred from depleted shergottites such as QUE 94201. The geophysical estimate of mantle radioactivity inferred here is a global average value, while values inferred from the martian meteorites are for particular points in the martian mantle. Evidently, the martian mantle has several isotopically distinct compositions, possibly including a radioactively enriched source that has not yet been sampled by the martian meteorites. The minimum mantle heating rate corresponds to a minimum thermal Rayleigh number of 2×10^6, implying that mantle convection remains moderately vigorous on present-day Mars. The basic convective pattern on Mars appears to have been stable for most of martian history, which has prevented the mantle flow from destroying the isotopic heterogeneity.

INTRODUCTION

Several lines of evidence indicate that volcanic activity has occurred on Mars in the geologically recent past. The shergottites are a class of igneous meteorite, the geochemistry of which indicates a martian origin (e.g., McSween and Treiman 1998). Many of the shergottites have radiometric ages of 180 Myr, although some are older (Nyquist et al. 2001). The Mars Orbital Camera on Mars Global Surveyor permits imaging of very small craters and has greatly improved our knowledge of young surface ages on Mars. At Olympus Mons and in Elysium Planitia, cratering studies indicate that some lava flows formed in the last 10–30 Myr (Hartmann and Neukum 2001). These cratering ages incorporate the current uncertainty in the cratering flux rate at Mars.

The existence of young volcanism on Mars implies that adiabatic decompression melting and, hence, upwelling convective flow in the mantle remains important on Mars at present. In this study, I model mantle convection and melt

production on present-day Mars. In particular, I test the sensitivity of the models to different choices of total radioactive heating rate and of the partitioning of radioactive elements between the mantle and crust. I also test the effects of varying the lithospheric thickness, the core-mantle boundary temperature, and the choice of solidus temperature. The primary observational constraint on the models is the requirement that successful models are able to generate at least some melting at present. This binary test (melt either occurs or does not occur) provides a strong constraint on the minimum amount of radioactive heating that remains in the mantle of Mars. Additional tests are provided by the spatial distribution of melting, the total melt production rate, and the mean melt fraction. The principal conclusion of this study is that the minimum average radioactive heating rate in the martian mantle at present is 1.6×10^{-12} W/kg, which corresponds to 39% of the total radioactivity of the Wänke and Dreibus (1994) composition model. This heating rate sets the minimum temperature and, thus, the maximum viscosity of the martian mantle. The minimum present-day thermal Rayleigh number is 2×10^6, implying that mantle convection on Mars remains at least moderately vigorous at present.

Previous studies of mantle convection and the thermal evolution of Mars have taken 2 different approaches. Studies of magma production on Mars have usually been performed using parameterized convection models (Spohn 1991; Breuer et al. 1993; Weizman et al. 2001; Hauck and Phillips 2002). Parameterized convection models assume a functional relationship between the vigor of convection, as measured by the Rayleigh number, and the efficiency of heat loss from the mantle. This allows the thermal evolution of a planet to be calculated by solving a system of ordinary differential equations. An important caveat is that such models are one-dimensional (vertical only) and, thus, yield only a solution for the average temperature as a function of depth. Because melting is limited to the highest temperatures in the mantle, parameterized convection calculations cannot be used to directly calculate magmatism on Mars. Previous studies have made arbitrary assumptions either about melting efficiency or about the magnitude of lateral temperature variations to estimate melting in the parameterized convection framework. In contrast to these earlier investigations, the current study explicitly solves for mantle temperature as a function of both horizontal and vertical location in the mantle. Thus, my results can be used directly with experimentally determined melting laws to calculate the expected magma production on Mars.

The second class of studies simulate mantle flow in either 2 or 3 dimensions and solve the complete set of partial differential equations that govern mantle convection (Schubert et al. 1990; Harder and Christensen 1996; Harder 1998, 2000; Breuer et al. 1997, 1998; Reese et al. 1998; Wüllner and Harder 1998; Zhong and Zuber 2001). Generally, these studies have not used magma production as a constraint on model results. Recently, Schott et al. (2001) considered magma production in a mantle convection simulation for Mars. Their model considered a very weak lithosphere and did not permit differentiation of radioactivity into the crust. These conditions are only relevant to the very earliest stage of martian history. Moreover, the melting relationships used in Schott's study were experimentally constrained only up to 1.5 GPa. In contrast, the simulations described here consider conditions appropriate for present-day Mars: a thick, strong lithosphere; up to 90% of the total radioactivity differentiated into the crust; and melting relationships that are experimentally constrained up to 9 GPa.

A CONCEPTUAL MODEL FOR THARSIS

Geologically recent volcanic activity has occurred in 2 general regions of Mars: Tharsis and Elysium (Scott and Tanaka 1986; Greeley and Guest 1987). The Tharsis rise is 4500 km across and reaches an elevation of 10 km. Three large shield volcanos, Arsia Mons, Pavonis Mons, and Ascraeus Mons, occupy the crest of Tharsis. Olympus Mons, the largest volcano in the solar system, is located on the northwest flank of Tharsis, and Alba Patera is on the north side of Tharsis. In addition, Tharsis also contains 7 smaller volcanos and vast lava plains (Hodges and Moore 1994). The Elysium rise, in the other hemisphere, is a small-scale version of Tharsis. Elysium is 1500 km across and reaches an elevation of 4 km. It includes 3 large shield volcanos and extensive regional lava plains (Hodges and Moore 1994; Mouginis-Mark and Yoshioka 1998).

Many investigators have treated Tharsis primarily as a region of volcanically thickened crust (e.g., Solomon and Head 1982; Phillips et al. 2001; Zhong 2002). Obviously, this must be true in part, but generation of the required volume of magma implies a hot mantle, which would contribute to the observed topographic uplift. The evidence cited in the Introduction for young volcanism on Mars indicates that convective upwelling and adiabatic decompression melting continues to be important, even on present-day Mars.

There are 2 fundamental types of energy source for driving convective flow in the mantle of Mars: bottom heating and internal heating (Davies 1999; Schubert et al. 2001). Bottom heating is heat that enters the base of the mantle from the core due to cooling of the core. Bottom heating produces a thin thermal boundary layer in the lowermost mantle just above the core-mantle boundary and, consequently, produces narrow, rising plumes in the mantle. Such plumes are thought to cause terrestrial hotspots such as Hawaii and Iceland (e.g., Morgan 1972; Watson and McKenzie 1991; Ito et al. 1999). Internal heating is due to radioactive decay within the mantle of Mars and to the release of specific heat as the mantle cools. Internal heating is not associated with a deep thermal boundary layer and produces broad convective upwellings and, hence, broad topographic rises (Davies 1999). On the

Earth, internal heating is the dominant energy source for driving mantle convection (e.g., Davies 1988; Sleep 1990).

These physical principles suggest the following schematic model for Tharsis. As on Earth, internal heating is likely to be the dominant energy source for mantle flow on Mars. The Tharsis topographic rise is at least partly due to convective uplift over a broad, internally heated convective upwelling. Embedded within this broad upwelling are several hot mantle plumes, which originate at the core-mantle boundary due to bottom heating. Each large volcano is (or was) fed by its own mantle plume. Because of the presence of the internally heated upwellings, the mantle beneath Tharsis and Elysium is warmer than the planetary average, and the mantle viscosity is lower than in other parts of Mars. Mantle plumes form when small-scale convective flow in the lower thermal boundary layer erupts upward into the overlying mantle (Olson et al. 1987). This occurs most readily in areas where the overlying mantle has a relatively low viscosity. Thus, the concentration of plume-driven volcanism in Tharsis and Elysium is a natural consequence of the broader, internally heated convection cells. A similar situation occurs on Earth, where hotspot volcanism occurs predominantly in seismically slow, hence warmer than average, mantle (Richards et al. 1988). Other researchers have sometimes considered Tharsis to be the surface expression of a single, broad mantle plume (e.g., Schubert et al. 1990; Harder and Christensen 1996). Such a description is misleading because it emphasizes the relatively minor bottom heating source and ignores the energetically more important internal heating. Also, the description of Tharsis as a single plume neglects the possibility that multiple plumes, each feeding a single large volcano, were active at any given time.

NUMERICAL METHODS

Mantle Convection Model

The numerical models in this study are based on the conceptual model outlined in the A Conceptual Model for Tharsis section. Both internal (radioactive) heating and bottom heating are included. The total amount of radioactive heating and its distribution between mantle and crust are specified in each model. The strength of the bottom heating is not specified directly but, instead, is determined by the temperature difference between the mantle and the core. The mantle's temperature is controlled in part by the magnitude and distribution of the radioactive heating. Models that retain most of the radioactivity in the mantle have high mantle temperatures and, thus, little heat flow out of the core. Models with most of the radioactivity in the crust have cooler mantles and, thus, a larger amount of heat flowing out of the core. In all of the models, the internal heating source is energetically dominant, just as is expected to occur on Mars. Because of the symmetry in the numerical models, only 1 mantle plume is present in the calculations. In the real Mars, it is possible (even likely) that more than one mantle plume was active in Tharsis at any given time.

The governing equations for convective flow in the mantle of Mars are conservation of mass for an incompressible fluid:

$$\nabla \cdot V = 0 \tag{1}$$

conservation of momentum:

$$-\nabla P + \nabla \cdot \tau + RaT\hat{\jmath} = 0 \tag{2}$$

and conservation of energy:

$$\frac{\partial T}{\partial t} + V \cdot \nabla T = \nabla^2 T + \frac{Ra_H}{Ra} \tag{3}$$

Here, V is the velocity, T is the temperature, P is the pressure, τ is the deviatoric stress tensor, t is time, and $\hat{\jmath}$ is a unit vector in the radial direction. These equations have been non-dimensionalized by scaling length by the mantle depth (d), temperature by the super-adiabatic temperature difference between the top and bottom of the mantle (ΔT), and time by the thermal diffusion time (d^2/κ), where κ is the thermal diffusivity (e.g., Kiefer and Kellogg 1998).

The solutions to this system of equations are governed by 2 Rayleigh numbers: the thermal Rayleigh number:

$$Ra = \frac{\rho_m g \alpha \Delta T d^3}{\kappa \eta} \tag{4}$$

and the internal heating Rayleigh number:

$$Ra_H = \frac{\rho_m g \alpha H d^5}{k \kappa \eta} \tag{5}$$

Here, ρ_m is the mantle density, g is the gravitational acceleration, α is the thermal expansion coefficient, η is the mantle viscosity, H is the volumetric internal heating rate, and k is the thermal conductivity. The value of Ra controls the overall vigor of convection, and the ratio of Ra_H and Ra (last term in Equation 3) controls the relative strength of internal and bottom heating. In the models presented here, the strength of the radioactive heating varies with depth, and so Ra_H is also depth-dependent. The numerical values for the various constants in Equations 4 and 5 are given in Table 1. Table 1 includes a nominal value for ΔT, although it is varied in a few models, as discussed in the Sensitivity to Core-Mantle Boundary Temperature section.

The mantle convection simulations were performed using finite element methods (Kellogg and King 1997). The momentum and continuity equations are solved using the penalty method and bilinear shape functions, while the energy equation is solved using the streamline-upwind Petrov-Galerkin method. Time stepping is done with an explicit,

Table 1. Scaling parameters.

Symbol	Property	Value	Reference
ρ_m	Mantle density	3400 kg m^{-3}	Bertka and Fei 1998
g	Gravitational acceleration	3.72 m s^{-2}	Yuan et al. 2001
α	Thermal expansion coefficient	3×10^{-5} K^{-1}	
ΔT	Vertical temperature contrast	1600°C	Sensitivity to Core-Mantle Boundary Temperature section
d	Depth of convecting layer	1698 km	Folkner et al. 1997
κ	Thermal diffusivity	10^{-6} m^2 s^{-1}	
k	Thermal conductivity	4 W m^{-1} K^{-1}	
ΔH_m	Latent heat of melting	6.4×10^5 J kg^{-1}	Navrotsky 1995
C_P	Specific heat	1200 J K^{-1} kg^{-1}	Navrotsky 1995
	Crust thickness	53 km	Zuber et al. 2000

second order accurate predictor-corrector algorithm, with the time step set to half of the Courant time step (Hughes 1987).

The results presented in this paper are calculated in an axisymmetric, hemispherical shell (see Fig. 1 of Kiefer and Kellogg [1998]). The non-hydrostatic geoid of Mars has a high degree of axial symmetry about Tharsis (Yuan et al. 2001). The geoid reflects a combination of density heterogeneity in the mantle (a direct measure of the present-day convective thermal structure) and regional variations in crustal thickness. Crustal thickness variations in Tharsis are presumably due to volcanism and, thus, reflect the integrated time history of convective upwelling and adiabatic decompression melting. Thus, assuming axisymmetry in the numerical models is a reasonable simplification. The computational grid is a hemispherical shell rather than a full spherical shell (see Fig. 3), thus reducing the computational costs. Because melting is restricted to a very small part of the model domain, restricting the model to a single hemisphere does not affect the melting results that are the primary focus of this study.

The non-dimensional inner radius of the model shell is at R = 1.0, and the outer radius is at R = 2.0. This corresponds to a dimensional core radius of 1698 km and a ratio of core radius to planetary radius of 0.5. For Earth, the corresponding ratio is 0.54. Only a few constraints presently exist for the size of the core of Mars. The mean planetary density and mean moment-of-inertia permit a broad range of core radii, ranging from 1200 to 1850 km for a moment-of-inertia of 0.366 (Schubert and Spohn 1990; Folkner et al. 1997; Harder 1998). Doppler tracking of Mars Global Surveyor has led to a recent determination of the k_2 Love number for solar tides, which, in turn, constrains the core radius to 1520–1840 km (Yoder et al. 2003). The core radius used in this study is in the middle of this range. For this core radius, the phase transition to the high pressure perovskite phase will not occur in the martian mantle (Bertka and Fei 1997). However, an independent determination of the tidal Love number is dramatically different (Smith et al. 2001), so the tidal Love number is probably not yet useful as a constraint on the interior structure of Mars.

The computational grid uses uniformly spaced elements in both coordinate directions, with 128 elements radially and 256 elements in colatitude. This corresponds to a vertical grid spacing of 13.3 km. The horizontal grid spacing varies between 10.4 km at the base of the mantle to 20.9 km at the surface. For the range of Rayleigh numbers used in this study, this grid provides excellent resolution of the thermal boundary layer structures. For comparison, the resolution used here is a factor of 2 to 5 better than that used in the melting study of Schott et al. (2001). The boundary conditions on the top and bottom surfaces of the shell are zero vertical velocity, zero shear stress, and constant temperature (T = 0 on the top and T = 1 on the bottom). The constant temperature boundary conditions allow heat to flow from the core into the base of the mantle and to escape from the crust to space. On the sides, the boundary conditions are zero lateral velocity, zero shear stress, and no lateral heat transport at the model pole (colatitude $\theta = 0$) and at the model equator ($\theta = \pi/2$).

Each model was initiated using a previous calculation as the starting condition. The adjustment to the new model conditions was monitored using time-series of surface heat flux and internal temperature. The transient adjustment period for each model is not included in the results described below. Figure 1 shows the evolution of the horizontally-averaged temperature at the mid-depth of the mantle for model 4. Because the radioactive heating rate is held constant in these models, Fig. 1 is not, strictly speaking, a time history for Mars. Rather, it shows the range of states that Mars could be in for this distribution of radioactivity. The absence of long-term secular heating or cooling of the mantle in this model demonstrates that the model has reached a statistical equilibrium with the imposed radioactive heating. Thermal history models for Mars show that the present-day mantle temperature is not sensitive to uncertainties in the initial formation temperature of Mars (Nimmo and Stevenson 2000; Weizman et al. 2001). Moreover, the low present-day mantle cooling rate in their models implies that Mars is close to thermal equilibrium. These results justify calculating the models in this paper to statistical equilibrium. The small-scale temperature fluctuations in Fig. 1 are due to the time-dependent evolution of thermal boundary layer instabilities (e.g., Kiefer and Kellogg 1998). In all of the results described in this paper, the models have been run for at least 20,000 time steps after the end of the transient adjustment period. This corresponds to a minimum time interval of 1 Gyr.

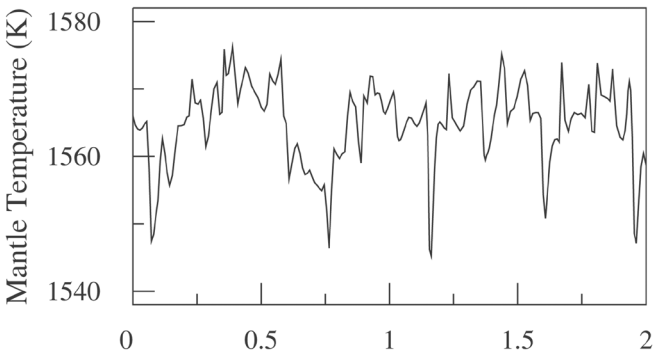

Fig. 1. The horizontally averaged temperature at the mid-depth of the mantle as a function of time for model 4. The absence of a long-term secular trend in the temperature indicates that the model has reached equilibrium with the imposed radioactive heating.

Radioactivity Models

The 2 most important parameters in these models are the total amount of radioactive heating and the partitioning of the radioactivity between the mantle and crust. Perhaps the most commonly used chemical composition model for Mars is the model of Wänke and Dreibus (1994, hereafter WD94), which is based on element correlations in the martian meteorites. An alternative approach is that of Lodders and Fegley (1997, hereafter LF97), who modeled Mars as a combination of CI, CV, and H chondrites. They adjusted the relative proportions of these meteorite classes to satisfy the oxygen isotope ratios observed in the martian meteorites. Table 2 shows the radioactive abundances for the bulk silicate Mars derived by these 2 approaches. The 2 major heat producing elements, uranium and thorium, are identical in the 2 models. On the other hand, potassium differs by a factor of 3 between the 2 models. At present, K makes only a minor contribution to the total radioactive heat production on Mars, so the LF97 model produces 1.5 times the present-day radioactive heating of the WD94 model. However, because of the short half-life of ^{40}K, the difference in heating rates was considerably larger early in martian history. McLennan (2001) showed that the K/U and K/Th ratios in the LF97 model are much higher than those observed in the martian meteorites or inferred from orbital gamma ray spectroscopy. Hauck and Phillips (2002) found that the LF97 model produces an excessively thick crust. In this paper, I emphasize models using the WD94 radioactivity but include some models for the LF97 radioactivity for completeness.

The partitioning of radioactivity between mantle and crust is the second key parameter of this study. I assume that from 30 to 90% of the total radioactive heating is partitioned into the crust. The mean crustal thickness on Mars is estimated to be approximately 50 km (Zuber et al. 2000; Nimmo and Stevenson 2001). In my numerical simulations, the crustal radioactive heating is uniformly distributed through a crust with a thickness of 53 km, corresponding to the upper 4 rows of elements in the grid. In this study, the crust is assumed to have a constant thickness. Wüllner and Harder (1998) explored the consequences of laterally variable crustal heat sources on mantle convection. The remaining heat sources are uniformly distributed throughout the mantle. Possible issues related to the non-uniform distribution of mantle heat sources are discussed in the Isotopic Reservoirs in the Martian Mantle section.

Table 2. Radioactivity models.

	Wänke[a]	Lodders[b]
K (ppm)	305	920
U (ppb)	16	16
Th (ppb)	56	56
Heating rate (10^{-12} W kg^{-1})	4.1	6.3

[a]Wänke and Dreibus (1994).
[b]Lodders and Fegley (1997).

Mantle Viscosity Model

The mantle viscosity in these models is a function of depth. To simulate the rheologic effects of the cold, near-surface thermal boundary layer, viscosity decreases exponentially with depth in the upper 212 km (the uppermost 16 rows of elements). The viscosity decreases by a factor of 10^5 from the surface to the base of this layer. This value of the viscosity contrast is large enough to put the models into the sluggish-lid or stagnant-lid mode of convection (Reese et al. 1998). In the Sensitivity to Lid Parameterization section, I show that this assumed value of the lid thickness is consistent with results derived from the gravity modeling of McGovern et al. (2002). Sensitivity tests for the choice of high viscosity lid thickness are also presented there.

Below the base of the high viscosity lid, the mantle viscosity is constant. The absolute viscosity of the mantle is calculated using a dry olivine rheology law (Chopra and Paterson 1984). The justification for assuming a dry mantle is discussed in the Melting Calculations section. The mantle viscosity is calculated using the horizontally averaged temperature at the mid-depth of the spherical shell, based on a characteristic mantle strain rate of 10^{-16} sec^{-1}. The mantle viscosity and, hence, the Rayleigh number were adjusted iteratively to assure self-consistency between the mantle viscosity and the assumed radioactive heating rate. For the models in this paper, the mantle viscosity varies between 3.5 $\times$ 10^{20} Pa-s (model 14) and 3.1 $\times$ 10^{21} Pa-s (model 11). Increasing the proportion of radioactivity that is partitioned into the crust causes a decrease in the average mantle temperature. This increases the mantle viscosity and, thus, decreases both Ra and Ra_H (see Table 3).

Melting Calculations

As is typical in mantle convection simulations, the model temperatures are initially determined in non-dimensional form with values between 0 and 1. To calculate the resulting

magma production, the non-dimensional temperature, T_{nd}, is converted to a dimensional temperature, T_{dim}, based on the relationship:

$$T_{dim} = T_S + T_{nd} \cdot \Delta T + Z \cdot T_{ad} \quad (6)$$

Here, T_S is the surface temperature (205 K). ΔT is the super-adiabatic temperature difference, the nominal value of which is assumed to be 1600 K. The effects of varying ΔT (or, equivalently, the core-mantle boundary temperature) are tested in the Sensitivity to Core-Mantle Boundary Temperature section. Z is the depth below the surface, and T_{ad} is the adiabatic gradient in the mantle, assumed to be 0.18 K/km.

The melting temperature of mantle materials is strongly affected by the presence or absence of water. A variety of evidence indicates that at least parts of the martian mantle are dry or nearly dry. Carr and Wänke (1992) found that the martian mantle has, at most, 18–36 ppm of water, based on measurements of water in Shergotty and assuming that it formed by 10–20% partial melting. Norman (1999) used rare earth element abundances to show that Shergotty formed by only 2–8% partial melting, with an optimal value of 4%, which would reduce the estimated source region water content to just 4–14 ppm, with an optimal value of 7 ppm. For comparison, the Earth's mid-ocean ridge basalt source region has 100–450 ppm water (Michael 1988; Sobolev and Chaussidon 1996). McSween et al. (2003) showed that the FeO-MgO-SiO_2 systematics of the basaltic shergottites and the nakhlites require formation under dry melting, tholeiitic conditions, although some other parts of the martian crust may require wet melting. Oxygen fugacity measurements provide additional constraints. Herd et al. (2001, 2002) determined oxygen fugacities for a number of shergottites using Fe-Ti oxide compositions. Wadhwa (2001) determined oxygen fugacities in shergottites from the oxidation state of europium in pyroxenes. Although some differences in detail exist, these studies agree that several shergottites, including QUE 94201, DaG 476, and lithology B of EET A79001, formed at very low oxygen fugacity, close to the iron-wustite buffer. These results do not permit the existence of free water in the mantle source region for these melts and, thus, imply that a dry solidus is appropriate. Preliminary results for SaU 094 and Dhofar 019 also indicate oxygen fugacities at or below the iron-wustite buffer (Herd 2002). Some other shergottites, such as Shergotty and Zagami, formed at higher fO_2 closer to the QFM buffer. These higher fO_2 values are usually interpreted as being due to contamination by water in the crust. Thus, dry melting is possibly appropriate for all shergottites. In contrast, Hauck and Phillips (2002) recently argued that wet melting was necessary to produce the observed crustal volume of Mars. They used the solidus for the terrestrial peridotite KLB-1. At high pressure, the KLB-1 solidus is hotter than either possible martian solidus considered in Fig. 2 (Wasserman et al. 2001). By considering one of the solidus curves in Fig. 2, reproducing the observed crustal thickness while still using a dry melting solidus might be possible. Overall, these results strongly suggest that many of the shergottites formed in an environment that is nearly water-free.

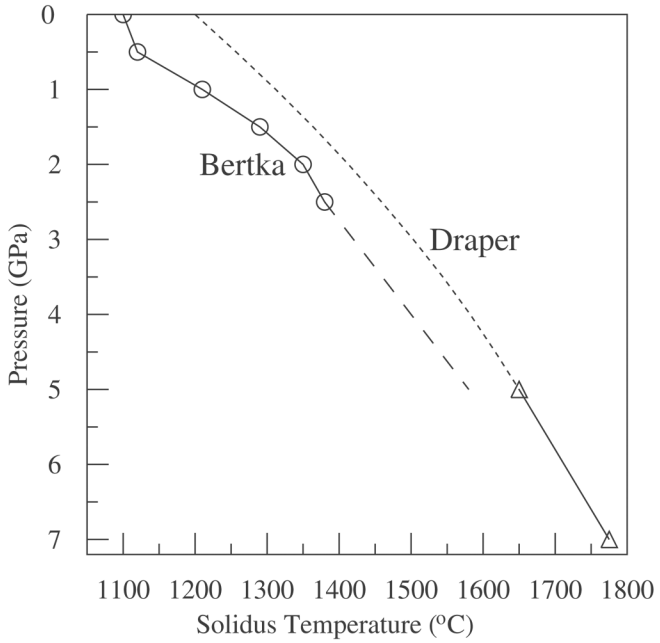

Fig. 2. The solidus temperature as a function of pressure for 2 Mars-analogue compositions. The circles and solid line are the results of Bertka and Holloway (1994), and the dashed line is an extrapolation to higher pressure. The triangles and solid line are the results of Draper et al. (2003) and Agee and Draper (Forthcoming), and the dotted line is an extrapolation to lower pressure.

In this study, therefore, I assume a dry solidus. Dry melting occurs at higher temperatures than wet melting and, thus, places much tighter constraints on the thermal structure of present-day Mars. Michael (1995), using data from Stolper and Newman (1994), estimated that water in the mid-ocean ridge basalt source region on Earth increases melting by no more than 1.5 wt% relative to the dry melting case. Applying this same approach to the lower water abundances on Mars, the Shergotty source region water would change the melt fraction by about 0.1 wt% and the total magma production rate by, at most, a few percent relative to a dry solidus. Thus, the results reported here are insensitive to the possible range of mantle water abundance.

Figure 2 shows the existing experimental constraints on the high pressure solidus of the martian mantle. Bertka and Holloway (1994) measured partial melting up to 3 GPa for the Wänke and Dreibus (1994) mantle composition. The circles show their experimental points, and the dashed line is a linear extrapolation of their results to higher pressures. Schmerr et al. (2001) measured melting for this same composition in the 15–25 GPa range. Although melting at these very high pressures does not occur on present-day Mars, the results may be useful in assessing melting and differentiation in very early Mars. Draper et al. (2003; D.

Draper, personal communication, 2002) and Agee and Draper (Forthcoming) studied melting at 5–9 GPa of the silicate portion of the Homestead L5 ordinary chondrite, the composition of which is similar to the estimated composition of the martian mantle. Their results are shown as triangles in Fig. 2. The dotted line is a quadratic extrapolation to lower pressure. One of the major goals of this study is to set a lower bound on the amount of radioactivity that must be present in the martian mantle to permit shergottite formation. For this reason, most of the results presented here are based on the Bertka and Holloway (1994) solidus, which is the lowest dry melting solidus available for a Mars-analogue composition. The sensitivity of the melting results to the choice of solidus temperature is assessed in the Sensitivity to Solidus Temperature section.

The melt production rate, M, is calculated from

$$M = \int \Gamma dV \tag{7}$$

where Γ is the differential melt production rate (Equation B1 of Watson and McKenzie [1991]) and the integral is over the portion of the mantle that is above the solidus temperature. Melting occurs only when Γ is increasing along the streamline of the flow. The integral is calculated numerically, with the contribution of each element in the grid being determined from the temperature, pressure, and flow velocity at the element center. As noted earlier, the convection models were performed in a hemispherical geometry rather than in a full sphere to reduce computational costs. Models performed in a full spherical shell would not necessarily produce equal melt volumes in the 2 hemispheres. Although both Tharsis and Elysium have been volcanically active in the geologically recent past (Hartmann and Neukum 2001), whether the 2 hemispheres of Mars have equal rates of present-day magma production is unclear. To be conservative, the melt production rates reported here are for a single model hemisphere.

Although the martian solidus is reasonably well-constrained (Fig. 2), unfortunately, no experimental constraints exist at present on the melt productivity above the solidus for a martian mantle composition at high pressure. Presumably, the melt productivity varies in a stepwise manner as each mineral phase is exhausted during the melting process. However, in the absence of specific constraints, I make the simple assumption that melt productivity is a linear function of temperature above the solidus. At 5 GPa, the martian solidus and liquidus are separated by about 200 K (Agee and Draper Forthcoming), so I assume a melt productivity of 0.5% per degree above the solidus (0.005 K^{-1}). A similar average melt productivity at 5 GPa was determined for the terrestrial peridotite KLB-1 by Takahashi et al. (1993). Uncertainties in the value of the melt productivity will map directly into the results for total melt production and for mean melt fraction. For example, when terrestrial peridotite is melted at 1 GPa, the melt productivity is very low just above the solidus and gradually increases with increasing temperature (Hirschmann et al. 1999). If a similar effect occurs at higher pressure, the actual melt production rates will probably be somewhat less than reported here.

For the melt production rates calculated in these models (see the Melt Production Rate section), the associated latent heat of melting is equivalent to less than 0.1% of the total global heat flux. Thus, the energy balance in the convection calculations (Equation 3) does not include the effects of latent heat of melting in calculating the mantle temperature structure. However, for the purpose of calculating the melt production, I modify the thermal field in the super-solidus region to account for the absorption of energy into the latent heat of melting:

$$\Delta T_m = X \cdot (\Delta H_m / C_P) \tag{8}$$

Here, X is the local melt fraction, and ΔT_m is the local change in mantle temperature required to balance the latent heat of melting, ΔH_m. Numerical values for ΔH_m and the specific heat, C_P, are given in Table 1, based on the compilation of Navrotsky (1995). The specific heat is based on an olivine and pyroxene bulk mantle composition, and the latent heat of melting is based on a basaltic melt composition.

RESULTS

I present results for a suite of 14 convection simulations. These models test the effects of varying the total amount of radioactivity, the fraction of radioactivity in the crust, the thickness of the near-surface high viscosity lid, the solidus temperature, and the temperature at the core-mantle boundary. Table 3 summarizes the model parameters and Table 4 summarizes the melting results for each model.

Table 3. Model parameters.

Model	Ra[a]	Ra_H[b]	Radioactive heating[c]	Crust fraction[d]	Lid thickness[e]
1	1.0×10^6	1.7×10^6	WD94	0.75	212
2	1.8×10^6	4.8×10^6	WD94	0.60	212
3	2.5×10^6	7.5×10^6	WD94	0.55	212
4	3.3×10^6	1.1×10^7	WD94	0.50	212
5	3.7×10^6	1.4×10^7	WD94	0.45	212
6	4.2×10^6	1.7×10^7	WD94	0.40	212
7	5.1×10^6	2.2×10^7	WD94	0.35	212
8	5.7×10^6	2.7×10^7	WD94	0.30	212
9	2.5×10^6	9.9×10^6	WD94	0.40	173
10	7.4×10^6	2.9×10^7	WD94	0.40	252
11	9.5×10^5	9.8×10^5	LF97	0.90	212
12	2.2×10^6	5.7×10^6	LF97	0.75	212
13	5.4×10^6	2.2×10^7	LF97	0.60	212
14	8.5×10^6	4.8×10^7	LF97	0.45	212

[a]Ra is the thermal Rayleigh number (Equation 4).
[b]Ra_H is the internal heating Rayleigh number (Equation 5).
[c]Radioactive heating indicates the radioactive heating model. WD94 is the Wänke and Dreibus (1994) radioactivity model. LF97 is the Lodders and Fegley (1997) radioactivity model.
[d]Crust fraction is the fraction of the total radioactivity that is partitioned into the crust (the upper 53 km of the model grid).
[e]Lid thickness is the thickness in km of the high viscosity, near-surface layer.

Table 4. Model results.

Model	Mean rate[a]	Maximum rate[b]	Time fraction[c]	Melt fraction[d]	Maximum fraction[e]
1	0.0	0.0	0.000	0.000	0.000
2	5.0×10^{-5}	6.2×10^{-3}	0.034	0.038	0.062
3	5.3×10^{-4}	2.7×10^{-2}	0.228	0.062	0.108
4	9.4×10^{-4}	2.5×10^{-2}	0.260	0.070	0.113
5	3.0×10^{-3}	2.2×10^{-2}	0.827	0.070	0.122
6	7.2×10^{-3}	5.7×10^{-2}	0.823	0.089	0.148
7	1.6×10^{-2}	9.4×10^{-2}	0.829	0.114	0.164
8	1.3×10^{-2}	8.1×10^{-2}	0.948	0.106	0.161
9	1.5×10^{-2}	7.7×10^{-2}	0.870	0.113	0.175
10	1.5×10^{-3}	4.5×10^{-2}	0.287	0.077	0.126
11	0.0	0.0	0.000	0.000	0.000
12	1.8×10^{-3}	1.3×10^{-2}	0.609	0.061	0.099
13	6.2×10^{-3}	6.2×10^{-2}	0.613	0.100	0.161
14	2.4×10^{-2}	1.4×10^{-1}	0.930	0.123	0.179

[a]Mean rate is the mean melt production rate in units of km^3 $year^{-1}$.
[b]Maximum rate is the maximum melt production rate in units of km^3 $year^{-1}$.
[c]Time fraction is the fraction of the simulation history that includes at least some melting.
[d]Melt fraction is the mean melt fraction produced in each model, averaged over time.
[e]Maximum fraction is the maximum melt fraction produced at any time in the simulation.

Mantle Temperature Fields

Changing the fraction of radioactivity that is in the crust of Mars has a strong influence on the temperature of the mantle and on the occurrence of present-day volcanism. Models 1–8 are based on the WD94 radioactivity model and systematically vary the fraction of radioactivity in the crust of Mars. If most of the radioactivity has been differentiated into the crust, the mantle is quite cold (model 1, Fig. 3a). On the other hand, retaining substantial amounts of radioactivity in the mantle allows the mantle to remain relatively warm (model 5, Fig. 3b).

Both temperature fields show the development of a strong, upwelling mantle plume. If melting does occur in these models, it is restricted to the hot head of these plumes. The temperature in the white region of Fig. 3b is above the Bertka and Holloway (1994) solidus. Melting occurs at depths of 240 to 305 km (2.9 to 3.8 GPa). No melting occurs in model 1. Although the core-mantle boundary temperature is identical in these 2 models, the cold mantle in Fig. 3a efficiently cools the plume as it rises. In the case of Fig. 3b, the warmer mantle allows the plume to retain sufficient heat to be able to melt when it approaches the surface. The observation that melting in these models is limited to hot mantle plume heads is consistent with the fact that recent volcanism on Mars is localized to a few small regions of the planet.

Melt Production Rate

Figure 4 shows the mean melt production rate as a function of the radioactive heating rate in the mantle. The triangles are for the WD94 models (models 2–8), and the squares are for the LF97 models (models 12–14). Increasing the mantle heating rate causes the mean mantle temperature to

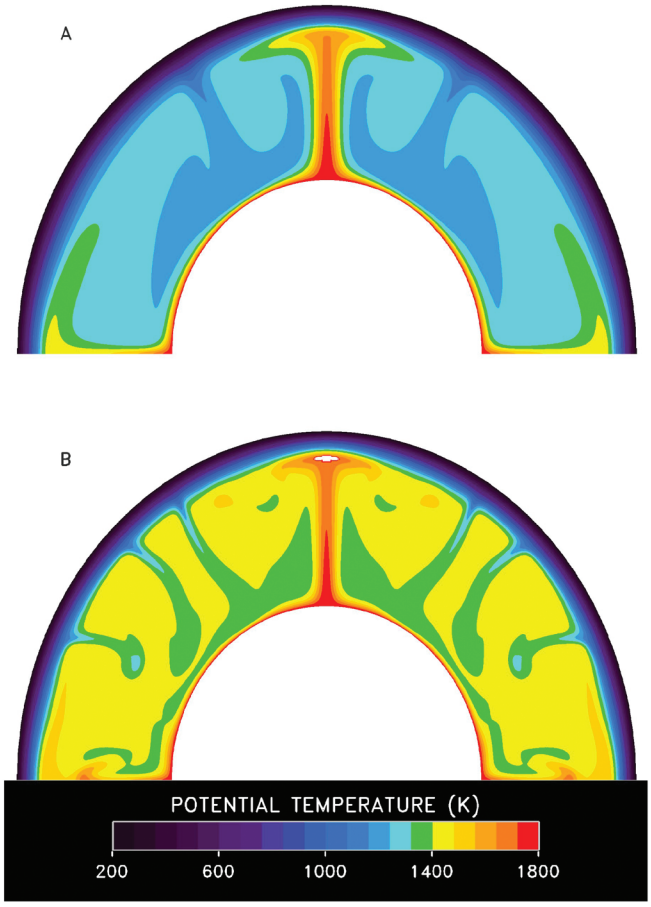

Fig. 3. a) The time-averaged thermal structure of model 1. The results are shown in terms of potential temperature, which is the physical temperature with the contribution of the adiabatic gradient removed (Equation 6); b) the potential temperature at 283 Ma for model 5. The region in white is above the Bertka and Holloway solidus. The complete melt production history for this model is shown in Fig. 5.

increase so that the hot plumes experience less cooling as they ascend from the base of the mantle. Thus, the melt production rate is a strongly increasing function of the mantle heating rate. At high mantle heating rates (>2.2×10^{-12} W/kg), most WD94 models (models 5, 6, and 8, solid line) lie close to the trend line defined by the LF97 models (dashed line). Model 7 produces an anomalously large amount of volcanism. This appears to be due to a relatively large separation between the central plume and the nearest cold downwelling in this particular model, so the plume cools less as it rises and, thus, produces more melt. At low mantle heating rates, much more crustal heating occurs in the LF97 models than in the WD94 models. This keeps the mantle warmer in the LF97 models, explaining the large difference in melt production at low mantle heating rates.

Tanaka et al. (1992) and Hartmann and Neukum (2001) have estimated that the volcanic resurfacing rate on Mars during the middle and late Amazonian, the most recent geologic epoch on Mars, is 10^{-2} km^2 $year^{-1}$. Because of the

low surface gravity, lava flows on Mars tend to be thicker than on Earth (Wilson and Head 1994). I assume typical flow thicknesses of 3 to 10 m, which is sufficient to obliterate the small craters that are used to date the ages of very young lava flows on Mars (Hartmann and Neukum 2001). I also assume that 5–20% of the magma produced in my models becomes extrusive lava flows, with the remaining magma forming intrusive magma bodies (Crisp 1984). With these assumptions, the horizontal long-dashed lines show the range of melt production rates (1.5×10^{-4} to 2×10^{-3} km^3 year^{-1}) that is consistent with the recent volcanic resurfacing history of Mars.

Model 2 produces magma just 3.4% of the time and, thus, effectively identifies the onset of volcanism for the WD94 models. For the WD94 models, the minimum mantle heating rate to produce any magmatism is 1.6×10^{-12} W/kg, which is 39% of the WD94 bulk silicate heating rate. The melt production rate matches the geologic observations if the mantle heating rate is between 1.8 and 2.1×10^{-12} W/kg. This corresponds to 43–50% of the WD94 radioactivity remaining in the mantle. None of the LF97 models shown in Fig. 4 are consistent with the geologically observed rate of volcanic resurfacing. The allowed rate of melt production is bracketed by model 11, which produces no melt, and model 12. This corresponds to a mantle heating rate of between 0.6 and 1.6×10^{-12} W/kg. However, because of the geochemical and geophysical objections to the LW97 model summarized in the Radioactivity Models section, I have not attempted to refine the LW97 melt production curve further.

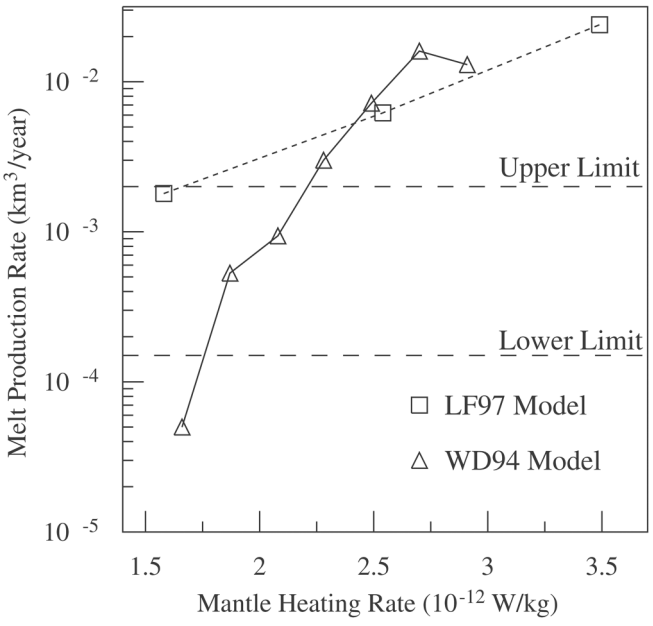

Fig. 4. The time-averaged melt production rate as a function of the radioactive heating rate in the mantle. The triangles and solid line are for models 2–8 and use the WD94 radioactivity model. The squares and short-dashed line are for models 12–14 and use the LF97 radioactivity model. The horizontal, long-dashed lines are geologically estimated bounds on the current rate of magma production on Mars, as discussed in the Melt Production Rate section.

The results in Fig. 4 are mean values averaged over the duration of each model calculation. The flow in each of these models is strongly time-dependent due to the development of thermal boundary layer instabilities (Kiefer and Kellogg 1998). This results in strong temporal variations in the magma production rate, illustrated in Fig. 5 for model 5. This model produces at least some magma 82% of the time and has a peak melt production rate that is 7 times the mean melt production rate. These characteristics are similar to those observed for other models with high mantle heating rates (Table 4). At lower mantle heating rates, magma is produced a smaller percentage of the time, as one would expect from the lower average temperature. The ratio of the maximum melt production rate to the mean melt production rate is highest for models with low amounts of mantle heating.

Schott et al. (2001) argued that temporal fluctuations in the amount of volcanic activity on Mars requires the presence of a feedback mechanism such as the use of a temperature- and pressure-dependent thermal conductivity. In fact, all of the models described in this paper are calculated using constant thermal conductivity. The time variability shown in Figs. 1 and 5 is due to the development of thermal boundary layer instabilities, which are expected processes at these Rayleigh numbers (e.g., Travis and Olson 1994; Kiefer and Kellogg 1998). Complex parameterizations of the thermal conductivity may contribute to the overall realism of the simulation but are not necessary to generate strongly episodic magmatism.

Melt Fraction

Figure 6 shows the calculated mean melt fractions for WD94 models 2–8. As one would expect, increasing the mantle heating rate causes an increase in the mean melt fraction. Based on a study of rare earth element concentrations and neodymium isotopes, Norman (1999) concluded that the shergottites formed by 2–8% partial melting of their source region. Borg et al. (1997) argued that

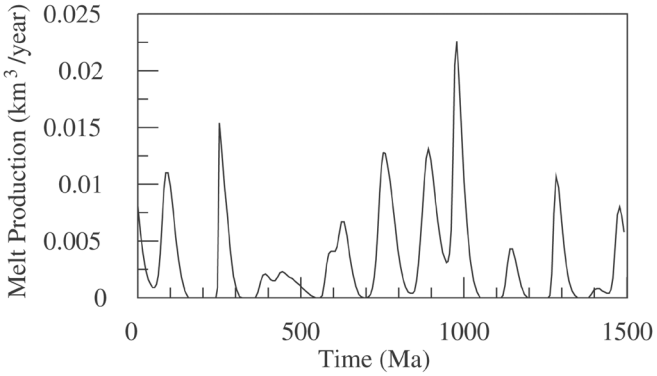

Fig. 5. The time variability of the melt production rate for model 5.

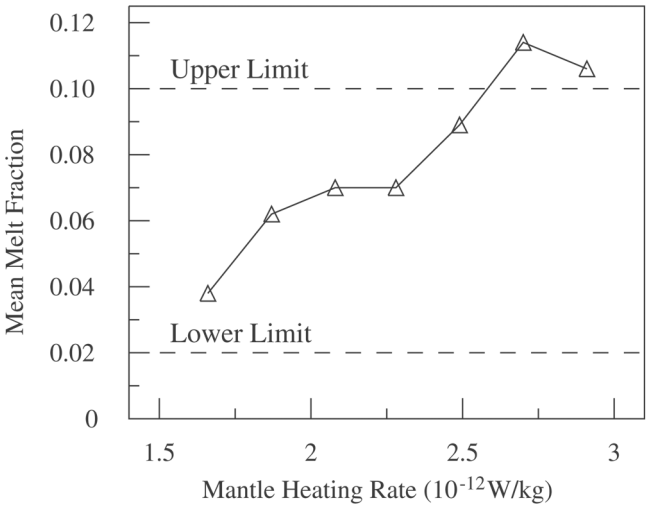

Fig. 6. The time-averaged mean melt fraction for models 2–8 as a function of the radioactive heating rate in the mantle. All of these models use the WD94 radioactivity model. The horizontal, long-dashed lines show the bounds on the observed melt fraction, as discussed in the Melt Fraction section.

QUE 94201 experienced 5 to 10 melting events, each on the order of 1%, with a total melting of 6–8%. Borg and Draper (2003) suggested that roughly 10% partial melting provides the best overall fit to the shergottite rare earth element data. The horizontal dashed lines in Fig. 6 show this range of partial melting. Figure 6 shows that a broad range of mantle heating rates are consistent with these constraints.

Because magma forms over a range of distances from the center of the plume, each model actually produces magmas with a range of melt fractions. As one way to characterize this, Table 4 shows both the mean melt fraction and the maximum melt fraction produced in each model. The maximum melt fractions are generally in the range of 11–18%, higher than the geochemical observations. However, these high melt fraction magmas are restricted to a small area in the center of the plume and usually to short episodes of unusually intense volcanism and, thus, are only a very small portion of the total magma production. As a result, unsurprisingly, the available collection of shergottites does not include any examples that formed at a very high melt fraction.

Sensitivity to Lid Parameterization

As discussed in the Mantle Viscosity Model section, the thickness of the near-surface, high viscosity lid in most of these simulations is assumed a priori to be 212 km. The high viscosity lid is a barrier to the ascent of mantle plume material and, thus, shuts off adiabatic decompression melting. Because the solidus temperature increases with pressure, the greatest amount of melting occurs at the lowest possible pressures, just below the base of the high viscosity layer. Thus, testing both the plausibility of the nominal lid thickness and the effects of varying this value is important.

McGovern et al. (2002) used gravity and topography data to determine the thickness of the elastic lithosphere at various locations on Mars. The base of the elastic lithosphere is controlled by the onset of ductile deformation and, thus, provides a constraint on the lithospheric thermal gradient and heat flux. McGovern et al. estimated heat fluxes at each of the 4 main Tharsis volcanos: Arsia, 15–33; Ascraeus, 14–26; Pavonis, 14–25; and Olympus, <18 mW m^{-2}. As a representative comparison, model 4 has a mean surface heat flux of 23.7 mW m^{-2} within a radius of 1000 km of the plume axis. The elastic support for the Tharsis volcanos comes primarily from the subcrustal lithosphere, so a better comparison between model and observation is probably the heat flux into the base of the crust. Again averaged out to a radius of 1000 km from the plume axis, model 4 has a heat flux of 17.8 mW m^{-2} into the base of the crust. Averaged in the same way, model 6 has a heat flux of 19.7 mW m^{-2} into the base of the crust.

Figure 7 illustrates how changing the lid thickness influences the resulting magmatism. Increasing the lid thickness from 173 km (model 9) to 252 km (model 10) decreases the average melt production rate by an order of magnitude (Fig. 7a). Increasing the lid thickness by a small additional amount (on the order of 20 km) will terminate melting altogether in this model. The mean melt fraction is also a strong function of lid thickness (Fig. 7b). The mean melt fraction for the 173 km thick lid exceeds the observational constraints. The melt fractions in the 212 km and 252 km-thick lid models are consistent with observations (Norman 1999; Borg and Draper 2003). Taken together, the magmatism results in Fig. 7 and the heat flux results suggest that a lid thickness of 200–250 km is appropriate for present-day Mars.

Sensitivity to Solidus Temperature

All of the melting results described so far have been based on the Bertka and Holloway (1994) solidus, which is the lowest temperature, dry melting solidus proposed for a Mars-analogue composition. Figure 2 shows that plausible changes in the assumed mantle composition can cause the solidus temperature to increase. Both of the solidus curves in Fig. 2 are for primitive mantle compositions. The present-day martian mantle should be somewhat depleted in the lowest melting point components, causing the solidus temperature to be higher. The mean crustal thickness on Mars is estimated to be about 50 km with an upper limit of 100 km (Zuber et al. 2000; Nimmo and Stevenson 2001), which corresponds to 4.3% of the planet's silicate mass. If the entire mantle is processed through the melting zone, on average, only a small amount of mantle melting (4–5%) is needed to produce the crust, so the average solidus should be perturbed upward only

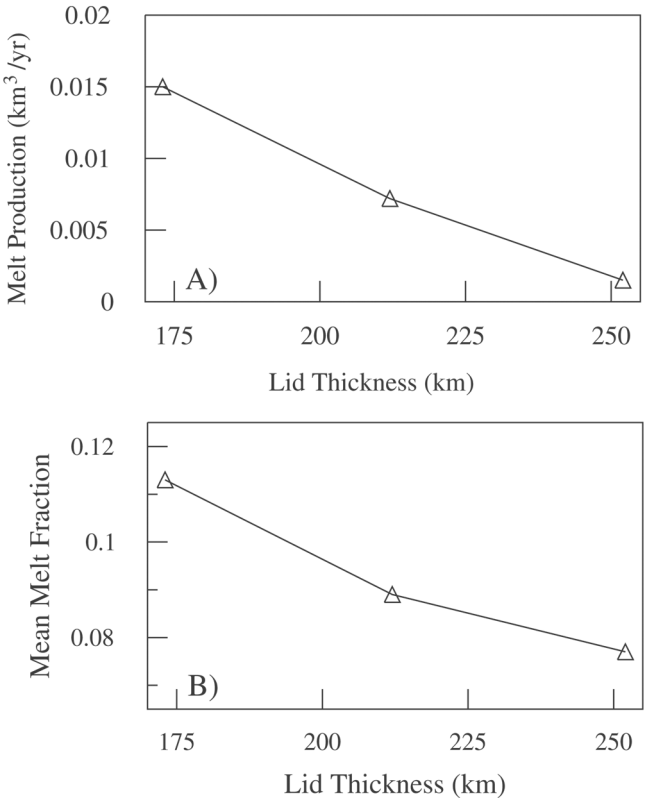

Fig. 7. a) The time-averaged melt production rate for models 6, 9, and 10 as a function of the assumed thickness of the high viscosity lid; b) the time-averaged mean melt fraction for models 6, 9, and 10 as a function of the assumed thickness of the high viscosity lid.

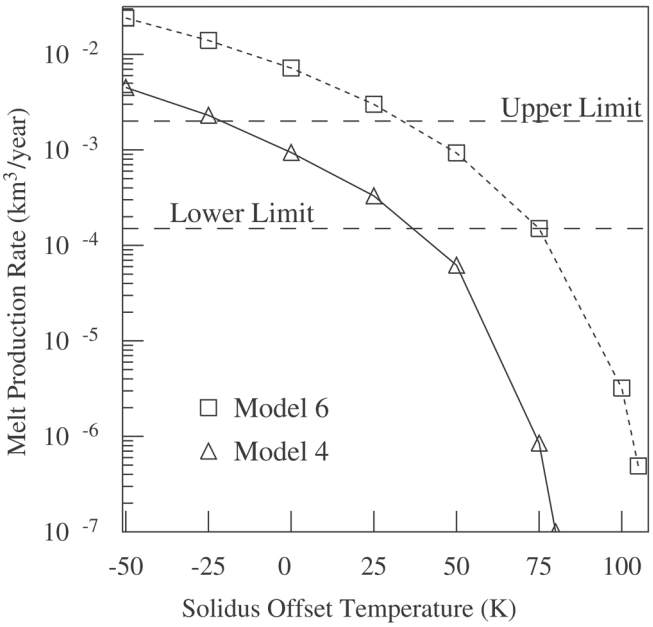

Fig. 8. Sensitivity of the melt production rate to the assumed mantle solidus. The solidus offset temperature is a linear offset relative to the Bertka and Holloway solidus. The triangles and solid line are results for the temperature offset applied to model 4. The squares and dotted line are results for the temperature offset applied to model 6. The horizontal, long-dashed lines are geologically estimated bounds on the current rate of magma production on Mars, as discussed in the Melt Production Rate section.

slightly from the values shown in Fig. 2. However, different parts of the mantle have likely experienced different degrees of previous melting. The specific source regions that melted to form the shergottites may have experienced either more or less melting than the mantle-wide average, so specifying a specific temperature increase for the depleted solidus in the shergottite source region is impossible. A second factor that contributes to uncertainty in the solidus temperature is the uncertainty in the martian mantle composition. Some composition models suggest that the FeO content of the martian mantle may be lower than assumed in Fig. 2 or, equivalently, that the Mg number must be increased (Ghosal et al. 1998; Agee and Draper Forthcoming). This would increase the solidus beyond the range shown in Fig. 2. Because of these 2 effects, assessing the effects of different solidus curves on the melting results is prudent.

Figure 8 shows melt production rates as a function of solidus temperature. The change in solidus temperature is applied as a constant offset relative to the Bertka and Holloway solidus, with positive offsets implying an increased solidus temperature. The Draper et al. (2003; Agee and Draper Forthcoming) solidus corresponds to an offset of about +70 K. The triangles are results for model 4, a WD94 model with 50% of the total radioactivity in the mantle. As expected, increasing the solidus offset temperature decreases the amount of melt produced. The long-dashed lines show the geologic bounds on melt production, as discussed for Fig. 4. Model 4 satisfies the required melt production for offset temperatures between −20 and +40 K. If the offset temperature is more than 80 K, no melting occurs in model 4. Larger offset temperatures can be accommodated by increasing the mantle heating rate. The squares show results for model 6, a WD94 model with 60% of the total radioactivity in the mantle. Model 6 produces the required amount of magma for a solidus offset temperature of up to +75 K. Melting ceases in model 6 if the offset temperature exceeds 105 K.

Sensitivity to Core-Mantle Boundary Temperature

In the numerical models, the super-adiabatic temperature contrast between the surface and the core-mantle boundary, ΔT, is an adjustable parameter. The surface temperature of Mars is known, so changing ΔT is equivalent to changing the temperature of the core-mantle boundary. This is an important parameter in this study because it sets the initial temperature of the rising plumes. Initially hot plume material has a better chance of melting when it approaches the surface. The core-mantle boundary temperature can be calculated from Equation 6 by setting the non-dimensional temperature

T_{ad} = 1 and the mantle depth Z = 1698 km. The nominal value of ΔT = 1600°C corresponds to a core-mantle boundary temperature of T_{CMB} = 1838°C.

An independent estimate of T_{CMB} comes from the thermal history modeling of Nimmo and Stevenson (2000), whose calculations include a range of initial temperatures and cooling modes. Their results were presented in terms of potential temperature. Therefore, I have added in the contribution from the adiabatic gradient (306°C) to compare their results with my simulations. Their estimated present-day core temperature is approximately 1800°C, slightly less than the nominal T_{CMB} assumed in this study. Nimmo and Stevenson (2000) also showed that the present-day value of T_{CMB} is not sensitive to reasonable changes in the assumed starting temperature 4.5 Gyr ago. If the martian core has a radioactive heat source due to ^{40}K (e.g., Murthy et al. 2003), T_{CMB} could be increased relative to the value calculated by Nimmo and Stevenson (2000).

Figure 9 illustrates the effects of changing T_{CMB}. Models 4 (triangles) and 6 (squares) have been rescaled for values of ΔT between 1525°C and 1650°C, corresponding to T_{CMB} between 1763°C and 1888°C. Changing T_{CMB} by 25°C changes the melt production rate by a factor of 2 to 5, with the largest effects occurring at the lowest values of T_{CMB}. The observed magmatism can be explained for T_{CMB} as low as 1760°C with mantle radioactivity of no more than 60% of the WD94 level (model 6).

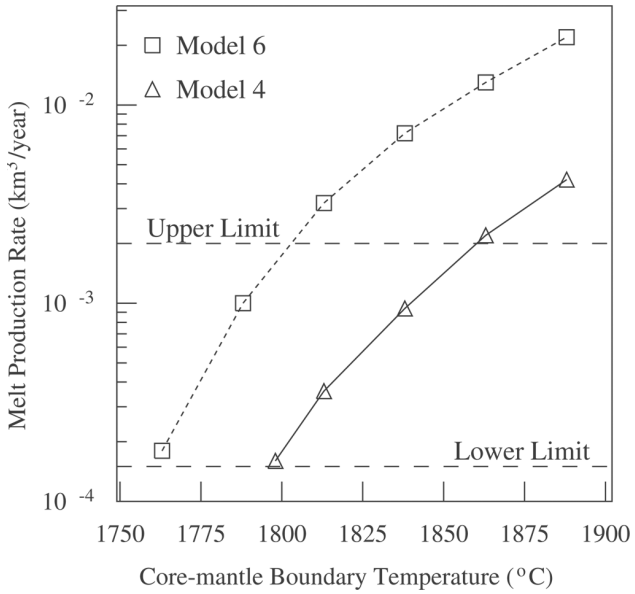

Fig. 9. Sensitivity of the melt production rate to the assumed core-mantle boundary temperature. The range of T_{CMB} shown here corresponds to values of ΔT between 1525 and 1650°C. The triangles and solid line are results for model 4. The squares and dotted line are results for model 6. The horizontal, long-dashed lines are geologically estimated bounds on the current rate of magma production on Mars, as discussed in the Melt Production Rate section.

Core Heat Flux and the Magnetic Dynamo

At present, Mars does not have a global magnetic field (Connerney et al. 2001) and, thus, does not have a magnetic dynamo operating in its core. One concern about the convection models reported here is that the heat flux out of the core is relatively high, 27–33 mW m^{-2}. The maximum conductive heat flux for the martian core is 19 mW m^{-2} (Nimmo and Stevenson 2000), so the core in these models must be convecting. In principle, this means that a dynamo could be present, although this is not guaranteed. Determining whether or not a dynamo actually occurs depends on the detailed dynamo mechanism and can be calculated in terms of a magnetic Reynolds number or dynamo number (Merrill et al. 1998). Detailed calculation of the dynamo number is beyond the scope of this paper.

Several mechanisms have been proposed for suppressing a magnetic dynamo on Mars. Nimmo and Stevenson (2000) invoke a change in the convective style of the mantle, which inhibits cooling of the mantle and causes the core and mantle to have virtually identical temperatures. This inhibits core convection and, thus, shuts off dynamo activity. However, their model is probably incompatible with the model described in this paper because the absence of a strong thermal boundary layer at the base of the mantle would prevent formation of mantle plumes in their model. Another possibility is that the liquid outer core is too thin to sustain dynamo activity (Stevenson 2001). A third possibility is that a blanket of hot material at the base of the mantle suppresses core convection. This is treated in more detail in the Isotopic Reservoirs in the Martian Mantle section.

DISCUSSION

Average Radioactive Element Content of the Martian Mantle

The results in this paper place important constraints on the average radioactive element content of the martian mantle. For the WD94 radioactivity model, a minimum mantle radioactive heating rate of 1.6 × 10^{-12} W/kg is needed to permit volcanism to occur at the present day, corresponding to 39% of the WD94 bulk silicate radioactivity remaining in the mantle. Geologic estimates of the recent volcanism rate are best matched by mantle heating rates of 1.8–2.1 × 10^{-12} W/kg, corresponding to 43–50% of the WD94 radioactivity remaining in the mantle. The most likely perturbations to the nominal parameter values assumed in these calculations are an increase in the solidus temperature or a decrease in the core-mantle boundary temperature. In either case, these changes can be compensated by increasing the amount of radioactivity retained in the mantle by roughly an additional 10%. Thus, for the WD94 radioactivity model, the mantle

must contain 50 ± 10% of the total radioactivity at the present day to explain the observed recent volcanism.

This degree of partitioning of radioactivity between the mantle and crust is geochemically plausible. As noted earlier, the crust is estimated to be 4.3% of the silicate mass of Mars. The shergottites formed as 2–10% partial melts (Norman 1999; Borg and Draper 2003). Most of the martian crust formed very early in martian history when the mantle was hotter, so a reasonable estimate is that the average crust formed as a 10% partial melt. Treating the radioactive elements as completely incompatible, this implies that 43% of the total radioactivity is now in the crust, with the remaining 57% in the mantle.

Isotopic Reservoirs in the Martian Mantle

Measurements of the martian meteorites provide a different perspective on the abundance of radioactive elements in the martian mantle. Several of the shergottites come from mantle source regions that are quite depleted in radioactive elements. One easy way to see this is to consider the abundance of thorium, which is thought to be relatively immobile during terrestrial weathering. Measured thorium abundances are less than 50 ppb in QUE 94201 (Lodders 1998), 11–25 ppb in DaG 476/489 (Folco et al. 2000; Barrat et al. 2001), and 40 ppb in Dhofar 019 (Taylor et al. 2002). Assuming that these meteorites formed due to 10% or less partial melting, this is equivalent to a Th abundance of no more than 1–5 ppb in the mantle source region. This is a factor of 10 to 50 less than the 56 ppb thorium abundance in the WD94 model.

Studies of radioactive isotopes show this result in a different way. Norman (1999) estimated that 51.5% of the total Nd in Mars is now in the crust, with the remaining 48.5% in the mantle. Depending on the mineral phase, U and Th are somewhat to substantially more incompatible than Nd (Jones 1995) and, thus, Norman's results may suggest that more than half of the U and Th should currently be in the martian crust. Borg et al. (1997) showed that the QUE 94201 source region was depleted by a factor of 15–60 in Nd, Sm, and Sr and was virtually depleted in Rb relative to the likely primitive mantle composition. Brandon et al. (2000) combined data from the Re-Os, Hf-W, and Sm-Nd systems to argue for the existence of either 2 or 3 isotopically distinct reservoirs in the martian mantle. Jones (2003) modeled the martian crust and mantle in terms of 3 isotopic reservoirs: a nakhlite source region with a radioactive heating rate of 1.6×10^{-12} W/kg, a highly depleted QUE 94201 source region with a radioactive heating rate of 6.2×10^{-13} W/kg, and an enriched crustal component. Borg (2002) proposed that the enriched component is another mantle reservoir rather than the crust.

Thus, we have a paradox: roughly half of the WD94 radioactivity must remain in the martian mantle to permit present-day magmatism, and yet, some of the shergottites apparently formed from source regions that are far more depleted in radioactivity than this. To resolve this paradox, one must recognize that the martian meteorites each represent a point measurement of chemical composition. Only a small number of martian meteorites are known, and the available data may not fully represent the compositional diversity of the martian mantle. On the other hand, the melting results presented here constrain the globally averaged mantle radioactivity and, thus, provide an integrated view of all of the various isotopic reservoirs. Figure 10 illustrates 2 possible models for isotopic reservoirs on Mars. Possibly, Mars includes aspects of both of these models. In the plum-pudding model (Fig. 10a), the background mantle is relatively high in radioactivity. For example, the nakhlite source region of Jones (2003) has the same radioactive heating rate as the minimum value derived here. The circles are more depleted reservoirs, similar to the QUE source region in Jones (2003). By embedding the low radioactivity QUE source region within a more radioactively enriched mantle, the depleted source region may be kept hot enough to melt in a mantle plume head. The blob-like distribution of depleted and primitive (or at least less-depleted) mantle in Fig. 10a may be a natural consequence of 4.5 Gyr of magmatic activity on Mars, with different regions of the mantle experiencing different amounts of melting and loss of incompatible elements to the crust. The differences between models with uniformly distributed mantle radioactivity (as modeled here) and models with

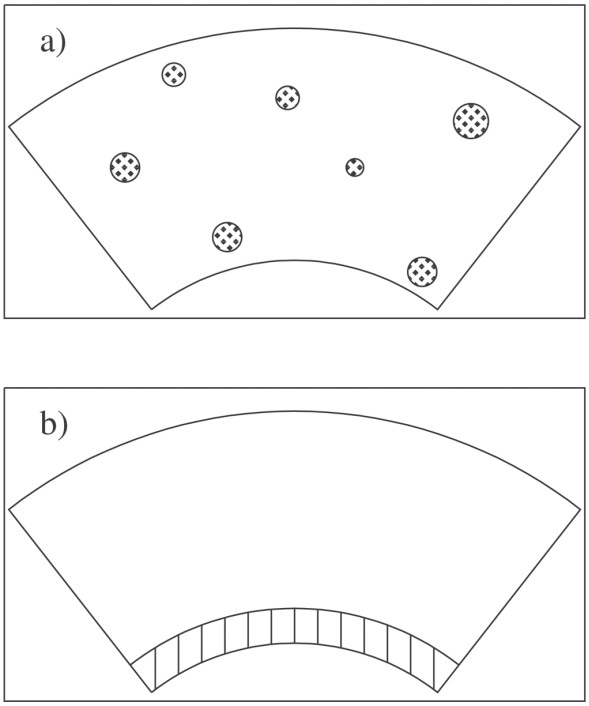

Fig. 10. Schematic distributions of radioactive reservoirs in the martian mantle: a) a plum-pudding distribution of enriched material (background) and depleted material (stippled circles); b) an enriched layer in the lowermost mantle (region filled with vertical lines) and a shallow depleted layer.

enriched and depleted blobs will depend on the spectrum of blob sizes. If the characteristic blob radius is similar to or smaller than a typical thermal diffusion length scale (say 100–200 km), the blob model and the uniform radioactivity model should have similar thermal structures and, thus, similar total melt production. Models with larger blobs are likely to diverge more from the results shown in this paper. Developing realistic models for this would be an important contribution to our understanding of the interior evolution of Mars but is likely to be computationally challenging.

The layered model (Fig. 10b) includes a deep layer that is enriched in radioactive elements and a more depleted shallow layer. This type of mantle layering might develop if Mars had an early, deep magma ocean (e.g., Righter et al. 1998). This layering resembles the models of Kellogg et al. (1999) and Coltice and Ricard (1999) for the Earth. The interface between the 2 mantle layers is shown here as occurring at a constant depth, although, if the density contrast between the 2 layers is small, substantial topographic relief can occur on the interface (Tackley 1998; Montague and Kellogg 2000). In assessing the plausibility of such layering, we must address 2 questions: 1) is the layering stable over geologic time?; and 2) can the deep layer hold enough radioactive elements? The long-term stability of such layering requires that the compositional density contrast between the 2 layers exceed the thermal buoyancy associated with hot, rising plumes. A density contrast of 3–6% is necessary (Kellogg and King 1993). Aluminum is a relatively refractory element and should be present on Mars in roughly chondritic abundance. The shergottite source region is depleted in aluminum (e.g., Longhi 1991). Although some of the missing Al is in the crust, the amount of Al depletion in the shergottite source region is too large to be explained by segregation of a basaltic crust alone (Longhi 2002). If the remaining Al is concentrated in a deep layer, garnet could provide the high density needed to stabilize the deep layer. However, high-pressure partitioning coefficients in garnet are a strong function of ionic radius (Draper et al. 2003), suggesting that garnet is unlikely to contain much U and Th. Some other phase that does contain U and Th would also need to be present. Both U and Th partition strongly into Ca-perovskites (Taura et al. 2001; Corgne and Wood 2002). Perovskite may be present in the deep layer if the mantle is thick enough and, thus, the pressure is high enough (Bertka and Fei 1997). If the deep layer contains sufficient radioactive elements, it may be hot enough to suppress heat flow out of the core and, thus, would prevent a magnetic dynamo from occurring at present. On the other hand, the hot layer could help power the mantle plumes that are necessary to explain present-day volcanism.

How Vigorous is Present-Day Mantle Convection on Mars?

The vigor of a convective flow is parameterized by its Rayleigh number (e.g., Davies 1999). The results in this paper constrain the minimum radioactive heating rate in the mantle and, thus, the minimum present-day mean mantle temperature. The mantle viscosity in these models and, thus, the Rayleigh numbers in Table 3 were adjusted to be self-consistent with the mantle temperature. Thus, the present-day thermal Rayleigh number (Equation 4) in the martian mantle is constrained to be at least 2×10^6 (model 2 of Table 3). This implies that mantle convection remains moderately vigorous on present-day Mars. For comparison, modeling of geoid anomalies and topographic uplift associated with mantle plumes indicates that the thermal Ra is in the range of 10^6 to 10^7 for Venus (Smrekar et al. 1997). The thermal Ra for whole mantle convection on Earth is about 10^7 based on a volumetrically averaged viscosity of 3×10^{21} Pa-s (Forte and Mitrovica 1996).

Mantle Convection and the Destruction of Isotopic Heterogeneity

Studies of isotopic systems with short half-lives indicate that strong isotopic heterogeneity, much larger than on Earth, has existed on Mars since it accreted. As a corollary, some conclude that Mars has not experienced significant mantle convection or else the isotopic heterogeneity would have been destroyed (e.g., Halliday et al. 2001). However, as shown here, mantle convection on Mars remains relatively vigorous even at the present day, and must have been still more vigorous in the past.

Convection inside Earth and Mars differs in 2 important ways that act to reduce the efficiency of convective mixing in the martian mantle. First, the planform of convection on Earth has varied strongly with time. In contrast, the convective planform on Mars has apparently been quite stable, with convective upwelling and volcanism centered beneath Tharsis and Elysium for much of martian history (e.g., Hodges and Moore 1994). The existence of relatively stable convection cell boundaries can inhibit mixing of material between convection cells (Schmalzl et al. 1996). Second, the presence of transform faulting in the Earth's plate tectonic style permits substantial toroidal motion (Lithgow-Bertelloni et al. 1993). In contrast, evidence for transform faulting on Mars does not exist. Toroidal motion can be visualized in simple terms as a horizontal swirling, which significantly increases the efficiency of convective mixing (Ferrachat and Ricard 1998; van Keken and Zhong 1999). Both of these factors permit isotopic heterogeneity to remain stronger in the martian mantle than on Earth.

Future Improvements

Several types of improvements are possible in future modeling. The present model uses depth-dependent viscosity to mimic the most important aspects of the stiff lithosphere. Models that use temperature-dependent viscosity are

computationally more expensive but would increase realism in 2 ways. First, low viscosity in the upwelling plume would permit a faster ascent velocity and, thus, less cooling in the plume. This may permit some relaxation of the minimum mantle radioactive heating rate inferred in this paper. Second, temperature-dependent viscosity would permit local thinning of the lithosphere at the center of the hot plume. This could increase both the magma production rate and the mean melt fraction. Another desirable addition to the numerical model would be to extend it to include earlier epochs in martian history. This would permit additional tests of the model, such as the total amount of crust produced during the history of Mars.

Improvements in the experimental petrology database would also help to refine the results in this paper. Particularly useful measurements would include: 1) measurements of the solidus curve for possible present-day, slightly depleted mantle compositions; and 2) measurements of the melt fraction as a function of temperature above the solidus, for both primitive and slightly depleted Mars mantle compositions. Both sets of measurements should be performed over a relatively broad pressure range. At present, melting occurs primarily in the range of 3–5 GPa. However, early in martian history, the mantle was hotter and the lithosphere was thinner, which would permit melting at both lower and higher pressures.

Spacecraft observations may also help in refining this work. Mars Odyssey includes a gamma ray spectrometer, which is currently measuring the distribution of K, U, and Th at the martian surface (Taylor et al. 2003). These observations measure only the composition of the upper few cm of the regolith. Measurements of the composition of ejecta deposits from large impact basins may provide some constraint on the radioactive concentrations as a function of depth, although this will be complicated by the large measurement footprint for the GRS data (several hundred km) and by the obscuring effects of aeolian dust. Seismic measurements by a lander network could constrain the crustal thickness in selected locations. Such measurements, in combination with existing gravity and topography data, would lead to a better estimate of the globally averaged crustal thickness. Together, these 2 sets of measurements would permit a better estimate of the total crustal radioactivity.

CONCLUSIONS

Both the radiometric ages of the shergottites and cratering statistics for lava flows in Tharsis and Elysium indicate that Mars has been volcanically active in the very recent past. This implies that adiabatic decompression melting and, hence, mantle convection on present-day Mars remains important. The numerical simulations presented in this paper show that for Mars to be volcanically active at present, the martian mantle must have retained 50 ± 10% of the Wänke and Dreibus (1994) radioactivity within the mantle. The quoted uncertainty incorporates reasonable uncertainties in the value of the solidus temperature and the core-mantle boundary temperature. This degree of partitioning of radioactivity between mantle and crust is a global average value and is geochemically reasonable for a 50 km thick crust formed by 10% partial melting. However, some shergottites show evidence of forming from a much more depleted mantle. Thus, the martian mantle must have several isotopically distinct compositions, arranged in either a plum-pudding fashion or in chemically isolated layers. The minimum present-day thermal Rayleigh number is 2×10^6, implying moderately vigorous mantle convection. The basic convective pattern on Mars appears to have been stable for most of martian history, which has prevented the mantle flow from destroying the isotopic heterogeneity.

Acknowledgments–Allan Treiman and John Jones inspired my interest in studying magma production on Mars and participated in many valuable discussions throughout this study. I thank Louise Kellogg for providing the finite element convection code, Connie Bertka and Dave Draper for discussions about high pressure melting relationships, and Chris Herd for discussions about the martian meteorites. Reviews by Mark Wieczorek, Kevin Righter, and an anonymous individual improved the clarity of the manuscript. I also thank Brian Fessler and Mike O'Dell for developing several very useful animations of the convection simulations. This work was carried out at the Lunar and Planetary Institute, which is run by the Universities Space Research Association under NASA Cooperative Agreement NCC5–679. Lunar and Planetary Institute Contribution 1196.

Editorial Handling—Dr. Kevin Righter

REFERENCES

Agee C. B. and Draper D. S. Forthcoming. Experimental constraints on the origin of martian meteorites and the composition of the martian mantle. *Earth and Planetary Science Letters.*

Barrat J. A., Blichert-Toft J., Nesbitt R. W., and Keller F. 2001. Bulk chemistry of Saharan shergottite Dar al Gani 476. *Meteoritics & Planetary Science* 36:23–29.

Bertka C. M. and Fei Y. 1997. Mineralogy of the martian interior up to core-mantle boundary pressures. *Journal of Geophysical Research* 102:5251–5264.

Bertka C. M. and Fei Y. 1998. Density profile of an SNC model martian interior and the moment-of-inertia factor. *Earth and Planetary Science Letters* 157:79–88.

Bertka C. M. and Holloway J. R. 1994. Anhydrous partial melting of an iron-rich mantle I: Subsolidus phase assemblages and partial melting phase relationships at 10 to 30 kbar. *Contributions to Mineralogy and Petrology* 115:313–322.

Borg L. E. 2002. Exploring trace element and isotopic mixing relationships in the martian meteorite suite (abstract). Workshop on Unmixing the SNCs: Chemical, Isotopic, and Petrologic Components of the Martian Meteorites. pp. 9–10.

Borg L. E. and Draper D. S. 2003. A petrological model for the origin of martian shergottite magmas based on their major element,

trace element, and isotopic composition (abstract #1169). 34th Lunar and Planetary Science Conference. CD-ROM.

Borg L. E., Nyquist L. E., Taylor L. A., Wiesmann H., and Shih C. Y. 1997. Constraints on martian differentiation processes from Rb-Sr and Sm-Nd isotopic analyses of the basaltic shergottite QUE 94201. *Geochimica et Cosmochimica Acta* 61:4915–4931.

Brandon A. D., Walker R. J., Morgan J. W., and Goles G. G. 2000. Re-Os isotopic evidence for early differentiation of the martian mantle. *Geochimica et Cosmochimica Acta* 64:4083–4095.

Breuer D., Spohn T., and Wüllner U. 1993. Mantle differentiation and the crustal dichotomy of Mars. *Planetary and Space Science* 41: 269–283.

Breuer D., Yuen D. A., and Spohn T. 1997. Phase transitions in the martian mantle: Implications for partially layered convection. *Earth and Planetary Science Letters* 148:457–469.

Breuer D., Yuen D. A., Spohn T., and Zhang S. 1998. Three-dimensional models of martian mantle convection with phase transitions. *Geophysical Research Letters* 25:229–232.

Carr M. H. and Wänke H. 1992. Earth and Mars: Water inventories as clues to accretional histories. *Icarus* 98:61–71.

Chopra P. N. and Paterson M. S. 1984. The role of water in the deformation of dunite. *Journal of Geophysical Research* 89: 7861–7876.

Coltice N. and Ricard Y. 1999. Geochemical observations and one layer mantle convection. *Earth and Planetary Science Letters* 174:125–137.

Connerney J. E. P., Acuña M. H., Wasilewski P. J., Kletetschka G., Ness N. F., Rème H., Lin R. P., and Mitchell D. L. 2001. The global magnetic field of Mars and implications for crustal evolution. *Geophysical Research Letters* 28:4015–4018.

Corgne A. and Wood B. J. 2002. $CaSiO_3$ and $CaTiO_3$ perovskite-melt partitioning of trace elements: Implications for gross mantle differentiation. *Geophysical Research Letters* 29:39-1–39-4.

Crisp J. A. 1984. Rates of magma emplacement and volcanic output. *Journal of Volcanology and Geothermal Research* 20:177–211.

Davies G. F. 1988. Ocean bathymetry and mantle convection 1. Large-scale flow and hotspots. *Journal of Geophysical Research* 93:10467–10480.

Davies G. F. 1999. *Dynamic Earth: Plates, plumes, and mantle convection.* New York: Cambridge University Press. 458 p.

Draper D. S., Xirouchakis D., and Agee C. B. 2003. Trace element partitioning between garnet and chondritic melt from 5 to 9 GPa: Implications for the onset of the majorite transition in the martian mantle. *Physics of the Earth and Planetary Interiors* 139:149–169.

Ferrachat S. and Ricard Y. 1998. Regular vs. chaotic mantle mixing. *Earth and Planetary Science Letters* 155:75–86.

Folco L., Franchi I. A., D'Orazio M., Rocchi S., and Schultz L. 2000. A new martian meteorite from the Sahara: The shergottite Dar al Gani 489. *Meteoritics & Planetary Science* 35:827–839.

Folkner W. M., Yoder C. F., Yuan D. N., Standish E. M., and Preston R. A. 1997. Interior structure and seasonal mass redistribution of Mars from radio tracking of Mars Pathfinder. *Science* 278:1749–1752.

Forte A. M. and Mitrovica J. X. 1996. New inferences of mantle viscosity from joint inversion of long-wavelength mantle convection and post-glacial rebound data. *Geophysical Research Letters* 23:1147–1150.

Ghosal S., Sack R. O., Ghiorso M. S., and Lipschutz M. E. 1998. Evidence for a reduced, Fe-depleted martian mantle source region of shergottites. *Contributions to Mineralogy and Petrology* 130:346–357.

Greeley R. and Guest J. E. 1987. Geologic map of the eastern equatorial region of Mars, Miscellaneous investigations map I-1802B. Washington D.C.: U.S. Geological Survey.

Halliday A. N., Wänke H., Birck J. L., and Clayton R. N. 2001. The accretion, composition, and early differentiation of Mars. *Space Science Reviews* 96:197–230.

Harder H. 1998. Phase transitions and the three-dimensional planform of thermal convection in the martian mantle. *Journal of Geophysical Research* 103:16775–16797.

Harder H. 2000. Mantle convection and the dynamic geoid of Mars. *Geophysical Research Letters* 27:301–304.

Harder H. and Christensen U. R. 1996. A one-plume model of martian mantle convection. *Nature* 380:507–509.

Hartmann W. K. and Neukum G. 2001. Cratering chronology and the evolution of Mars. *Space Science Reviews* 96:165–194.

Hauck S. A. and Phillips R. J. 2002. Thermal and crustal evolution of Mars. *Journal of Geophysical Research* 107, doi: 10.1029/2001JE001801.

Herd C. D. K. 2002. Martian basalt oxygen fugacity and geochemistry: Implications for a heterogeneous mantle (abstract). Workshop on Unmixing the SNCs: Chemical, Isotopic, and Petrologic Components of the Martian Meteorites. pp. 21–22.

Herd C. D. K., Papike J. J., and Brearly A. J. 2001. Oxygen fugacity of martian basalts from electron microprobe oxygen and TEM-EELS analyses of Fe-Ti oxides. *American Mineralogist* 86: 1015–1024.

Herd C. D. K., Borg L. E., Jones J. H., and Papike J. J. 2002. Oxygen fugacity and geochemical variations in the martian basalts: Implications for martian basalt petrogenesis and the oxidation state of the upper mantle of Mars. *Geochimica et Cosmochimica Acta* 66:2025–2036.

Hirschmann M. M., Asimow P. D., Ghiorso M. S., and Stolper E. M. 1999. Calculation of peridotite partial melting from thermodynamic models of minerals and melts. III. Controls on isobaric melt production and the effect of water on melt production. *Journal of Petrology* 40:831–851.

Hodges C. A. and Moore H. J. 1994. *Atlas of volcanic landforms on Mars.* Professional paper 1534. Washington D.C.: U.S. Geological Survey. 194 p.

Hughes T. J. R. 1987. *The finite element method: Linear static and dynamic finite element analysis.* Englewood Cliffs: Prentice Hall. 803 p.

Ito G., Shen Y., Hirth G., and Wolfe C. J. 1999. Mantle flow, melting, and dehydration melting of the Iceland mantle plume. *Earth and Planetary Science Letters* 165:81–96.

Jones J. H. 1995. Experimental trace element partitioning. In *Rock physics and phase relations: A handbook of physical constants,* edited by Ahrens T. J. Washington D.C.: American Geophysical Union. pp. 73–104.

Jones J. H. 2003. Constraints on the structure of the martian interior determined from the chemical and isotopic systematics of SNC meteorites. *Meteoritics & Planetary Science.* This issue.

Kellogg L. H. and King S. D. 1993. Effect of mantle plumes on the growth of D" by reaction between the core and mantle. *Geophysical Research Letters* 20:379–382.

Kellogg L. H. and King S. D. 1997. The effect of temperature-dependent viscosity on the structure of new plumes in the mantle: Results of a finite element model in a spherical axisymmetric shell. *Earth and Planetary Science Letters* 148:13–26.

Kellogg L. H., Hager B. H., and van der Hilst R. D. 1999. Compositional stratification in the deep mantle. *Science* 283: 1881–1884.

Kiefer W. S. and Kellogg L. H. 1998. Geoid anomalies and dynamic topography from time-dependent, spherical axisymmetric mantle convection. *Physics of the Earth and Planetary Interiors* 106: 237–256.

Lithgow-Bertelloni C., Richards M. A., Ricard Y., O'Connell R. J.,

and Engebretson D. C. 1993. Toroidal-poloidal partitioning of plate motions since 120 Ma. *Geophysical Research Letters* 20: 375–378.

Lodders K. 1998. A survey of shergottite, nakhlite, and Chassigny meteorites whole rock compositions. *Meteoritics & Planetary Science* 33:A183–A190.

Lodders K. and Fegley B. 1997. An oxygen isotope model for the composition of Mars. *Icarus* 126:373–394.

Longhi J. 1991. Complex magmatic processes on Mars: Inferences from the SNC meteorites. Proceedings, 21st Lunar and Planetary Science Conference. pp. 695–709.

Longhi J. 2002. SNC meteorites and their source composition(s) (abstract). Workshop on Unmixing the SNCs: Chemical, Isotopic and Petrologic Components of the Martian Meteorites. pp. 33–34.

McGovern P. J., Solomon S. C., Smith D. E., Zuber M. T., Simons M., Wieczorek M. A., Phillips R. J., Neumann G. A., Aharonson O., and Head J. W. 2002. Localized gravity/topography admittance and correlation spectra on Mars: Implications for regional and global evolution. *Journal of Geophysical Research* 107, doi: 10.1029/2002JE001854.

McLennan S. M. 2001. Crustal heat production and the thermal evolution of Mars. *Geophysical Research Letters* 28:4019–4022.

McSween H. Y. and Treiman A. H. 1998. Martian meteorites. In *Planetary materials,* edited by Papike J. J. Washington D.C.: Mineralogical Society of America. pp. 6-1–6-53.

McSween H. Y., Grove T. L., and Wyatt M. B. 2003. Constraints on the composition and petrogenesis of the martian crust. Journal of Geophysical Research 108, doi: 10.1029/2003JE002175.

Merrill R. T., McElhinny M. W., and McFadden P. L. 1998. *The magnetic field of the Earth: Paleomagnetism, the core, and the deep mantle.* New York: Academic Press. p. 527.

Michael P. J. 1988. The concentration, behavior, and storage of H_2O in the suboceanic upper mantle: Implications for mantle metasomatism. *Geochimica et Cosmochimica Acta* 52:555–566.

Michael P. J. 1995. Regionally distinctive sources of depleted MORB: Evidence from trace elements and H_2O. *Earth and Planetary Science Letters* 131:301–320.

Montague N. L. and Kellogg L. H. 2000. Numerical models of a dense layer at the base of the mantle and implications for the geodynamics of D". *Journal of Geophysical Research* 105: 11101–11114.

Morgan W. J. 1972. Plate motions and deep mantle convection. *Geological Society of America Memoir* 132:7–22.

Mouginis-Mark P. and Yoshioka M. T. 1998. The long lava flows of Elysium Planitia, Mars. *Journal of Geophysical Research* 103: 19389–19400.

Murthy V. R., van Westrenen W., and Fei Y. 2003. Experimental evidence that potassium is a substantial radioactive heat source in planetary cores. *Nature* 423:163–165.

Navrotsky A. 1995. Thermodynamic properties of minerals. In *Mineral physics and crystallography: A handbook of physical constants,* edited by Ahrens T. J. Washington D.C.: American Geophysical Union. pp. 18–28.

Nimmo F. and Stevenson D. J. 2000. Influence of early plate tectonics on the thermal evolution and magnetic field of Mars. *Journal of Geophysical Research* 105:11969–11979.

Nimmo F. and Stevenson D. J. 2001. Estimates of martian crustal thickness from viscous relaxation of topography. *Journal of Geophysical Research* 106:5085–5098.

Norman M. D. 1999. The composition and thickness of the crust of Mars estimated from rare earth elements and neodymium-isotopic compositions of martian meteorites. *Meteoritics & Planetary Science* 34:439–449.

Nyquist L. E., Bogard D. D., Shih C. Y., Greshake A., Stöffler D., and Eugster O. 2001. Ages and geologic histories of martian meteorites. *Space Science Reviews* 96:105–164.

Olson P., Schubert G., and Anderson C. 1987. Plume formation in the D"-layer and the roughness of the core-mantle boundary. *Nature* 327:409–413.

Phillips, R. J., Zuber M. T., Solomon S. C., Golombek M. P., Jakosky B. M., Banerdt W. B., Smith D. E., Williams R. M. E., Hynek B. M., Aharonson O., and Hauck S. A. 2001. Ancient geodynamics and global-scale hydrology on Mars. *Science* 291:2587–2591.

Reese C. C., Solomatov V. S., and Moresi L. N. 1998. Heat transport efficiency for stagnant lid convection with dislocation viscosity: Application to Mars and Venus. *Journal of Geophysical Research* 103:13643–13657.

Richards M. A., Hager B. H., and Sleep N. H. 1988. Dynamically supported geoid highs over hotspots: Observation and theory. *Journal of Geophysical Research* 93:7690–7708.

Righter K., Hervig R. L., and Kring D. A. 1998. Accretion and core formation on Mars: Molybdenum contents of melt inclusion glasses in three SNC meteorites. *Geochimica et Cosmochimica Acta* 62:2167–2177.

Schmalzl J., Houseman G. A., and Hansen U. 1996. Mixing in vigorous, time-dependent three-dimensional convection and application to Earth's mantle. *Journal of Geophysical Research* 101:21847–21858.

Schmerr N. C., Fei Y., and Bertka C. 2001. Extending the solidus for a model iron-rich martian mantle composition to 25 GPa (abstract #1157). 32nd Lunar and Planetary Science Conference. CD-ROM.

Schott B., van den Berg A. P., and Yuen D. A. 2001. Focused time-dependent martian volcanism from chemical differentiation coupled with variable thermal conductivity. *Geophysical Research Letters* 28:4271–4274.

Schubert G. and Spohn T. 1990. Thermal history of Mars and the sulfur content of its core. *Journal of Geophysical Research* 95: 14095–14104.

Schubert G., Bercovici D., and Glatzmaier G. A. 1990. Mantle dynamics in Mars and Venus: Influence of an immobile lithosphere on three-dimensional mantle convection. *Journal of Geophysical Research* 95:14105–14129.

Schubert G., Turcotte D. L., and Olson P. 2001. *Mantle convection in the Earth and planets.* New York: Cambridge University Press. 940 p.

Scott D. H. and Tanaka K. L. 1986. Geologic map of the western equatorial region of Mars, Miscellaneous investigations map I-1802A. Washington D.C.: U.S. Geological Survey.

Sleep N. H. 1990. Hotspots and mantle plumes: Some phenomenology. *Journal of Geophysical Research* 95:6715–6736.

Smith D. E., Zuber M. T., and Neumann G. A. 2001. Seasonal variation of snow depth on Mars. *Science* 294:2141–2146.

Smrekar S. E., Kiefer W. S., and Stofan E. R. 1997. Large volcanic rises on Venus. In *Venus II: Geology, geophysics, atmosphere and solar wind environment,* edited by Bougher S. W., Hunten D. M., and Phillips R. J. Tucson: University of Arizona Press. pp. 845–878.

Sobolev A. V. and Chaussidon M. 1996. H_2O concentrations in primary melts from supra-subduction zones and mid-ocean ridges: Implications for H_2O storage and recycling in the mantle. *Earth and Planetary Science Letters* 137:45–55.

Solomon S. C. and Head J. W. 1982. Evolution of the Tharsis province of Mars: The importance of heterogeneous lithospheric thickness and volcanic construction. *Journal of Geophysical Research* 87:9755–9774.

Spohn T. 1991. Mantle differentiation and thermal evolution of Mars, Mercury, and Venus. *Icarus* 90:222–236.

Stevenson D. J. 2001. Mars' core and magnetism. *Nature* 412:214–219.

Stolper E. and Newman S. 1994. The role of water in the petrogenesis of Mariana trough magmas. *Earth and Planetary Science Letters* 121:293–325.

Tackley P. J. 1998. Three-dimensional simulations of mantle convection with a thermo-chemical basal boundary layer: D”? In *The core-mantle boundary region,* edited by Gurnis M., Wysession M. E., Knittle E., and Buffet B. A. Washington D.C.: American Geophysical Union. pp. 231–253.

Takahashi E., Shimazaki T., Tsuzaki Y., and Yoshida H. 1993. Melting study of a peridotite KLB-1 to 6.5 GPa and the origin of basaltic magmas. *Philosophical Transactions of the Royal Society of London A* 342:105–120.

Tanaka K. L., Scott D. H., and Greeley R. 1992. Global stratigraphy. In *Mars,* edited by Kieffer H. H., Jakosky B. M., Snyder C. W., and Matthews M. S. Tucson: University of Arizona Press. pp. 345–382.

Taura H., Yurimoto H., Kato T., and Sueno S. 2001. Trace element partitioning between silicate perovskites and ultracalcic melt. *Physics of the Earth and Planetary Interiors* 124:25–32.

Taylor G. J., Boynton W., Hamara D., Kerry K., Janes D., Keller J., Feldman W., Prettyman T., Reedy R., Brückner J., Wänke H., Evans L., Starr R., Squyres S., Karunatillake S., Gasnault O., and Odyssey GRS Team. 2003. Igneous and aqueous processes on Mars: Evidence from measurements of K and Th by the Mars Odyssey Gamma Ray Spectrometer (abstract #3207). Sixth International Conference on Mars. CD-ROM.

Taylor L. A., Nazarov M. A., Shearer C. K., McSween H. Y., Cahill J., Neal C. R., Ivanova M. A., Barsukova L. D., Lentz R. C., Clayton R. N., and Mayeda T. K. 2002. Martian meteorite Dhofar 019: A new shergottite. *Meteoritics & Planetary Science* 37: 1107–1128.

Travis B. and Olson P. 1994. Convection with internal heat sources and thermal turbulence in the Earth’s mantle. *Geophysical Journal International* 118:1–19.

van Keken P. and Zhong S. 1999. Mixing in a 3D spherical model of present-day mantle convection. *Earth and Planetary Science Letters* 171:533–547.

Wadhwa M. 2001. Redox state of Mars’ upper mantle and crust from Eu anomalies in shergottite pyroxenes. *Science* 291:1527–1530.

Wänke H. and Dreibus G. 1994. Chemistry and accretion history of Mars. *Philosophical Transactions of the Royal Society of London A* 349:285–293.

Wasserman A. A., Chabot N. L., Draper D. S., and Agee C. B. 2001. High pressure anhydrous phase relations of Homestead L5: An analogue for the martian mantle (abstract #2029). 32nd Lunar and Planetary Science Conference. CD-ROM.

Watson S. and McKenzie D. 1991. Melt generation by plumes: A study of Hawaiian volcanism. *Journal of Petrology* 32:501–537.

Weizman A., Stevenson D. J., Prialnik D., and Podolak M. 2001. Modeling the volcanism of Mars. *Icarus* 150:195–205.

Wilson L. and Head J. W. 1994. Mars: Review and analysis of volcanic eruption theory and relationships to observed landforms. *Reviews of Geophysics* 32:221–263.

Wüllner U. and Harder H. 1998. Convection underneath a crust inhomogeneously enriched in heat sources: Application to martian mantle dynamics. *Physics of the Earth and Planetary Interiors* 109:129–150.

Yoder C. F., Konopliv A. S., Yuan D. N., Standish E. M., and Folkner W. M. 2003. Fluid core size of Mars from detection of the solar tide. *Science* 300:299–303.

Yuan D. N., Sjogren W. L., Konopliv A. S., and Kucsinskas A. B. 2001. Gravity field of Mars: A 75th degree and order model. *Journal of Geophysical Research* 106:23377–23401.

Zhong S. 2002. Effects of lithosphere on the long-wavelength gravity anomalies and their implications for the formation of the Tharsis rise on Mars. *Journal of Geophysical Research* 107, doi: 10.1029/2001JE001589.

Zhong S. and Zuber M. T. 2001. Degree-1 mantle convection and the crustal dichotomy on Mars. *Earth and Planetary Science Letters* 189:75–84.

Zuber M. T., Solomon S. C., Phillips R. J., Smith D. E., Tyler G. L., Aharonson O., Balmino G., Banerdt W. B., Head J. W., Johnson C. L., Lemoine F. G., McGovern P. J., Neumann G. A., Rowlands D. D., and Zhong S. 2000. Internal structure and early thermal evolution of Mars from Mars Global Surveyor topography and gravity. *Science* 287:1788–1793.